JOURNAL OF CATALYSIS 157, 14–24 (1995)

Autonomous Kinetic Oscillations during NO + C_2H_4 + O_2 Reaction over Pt–ZSM-5 under Highly Oxidizing Conditions

Byong K. Cho,[1] Jae E. Yie,[2] and Kenneth M. Rahmoeller

Physical Chemistry Department, General Motors Research & Development Center, Warren, Michigan 48090-9055

Received August 9, 1994; revised July 10, 1995; accepted July 24, 1995

This work has investigated, using a packed-bed laboratory reactor, the steady-state behavior of a Pt–ZSM-5 catalyst for the NO + C_2H_4 + O_2 reaction under highly oxidizing conditions, typical of lean-burn gasoline engine exhaust. Results have revealed very unusual kinetic behavior near the reaction lightoff temperature. For the first time, we have observed sustained kinetic oscillations, induced by the presence of NO, in the steady-state rate of the NO + C_2H_4 + O_2 reaction. The pattern of the oscillation was found to be very sensitive to catalyst temperature and feed composition. The steady-state rate of the NO + C_2H_4 + O_2 reaction is inhibited by NO and exhibits a strong kinetic isotope effect; the inhibition effect of ^{15}NO is much greater than that of ^{14}NO. Possible mechanisms of the observed kinetic oscillations are discussed on the basis of both the kinetic inhibition effect of NO on the catalytic surface and the surface phase transition of Pt induced by adsorbed NO.

INTRODUCTION

Because of its importance in controlling exhaust emissions from lean-burn gasoline and diesel-powered engines as well as from stationary power plants fueled by natural gas, catalytic reduction of NO by hydrocarbons in the presence of excess oxygen has been extensively investigated recently over the world (1–26). Since the pioneering work of Iwamoto *et al.* (27), Cu–ZSM-5 has been widely recognized as the most promising "lean NO_x catalyst," although Pt–ZSM-5 has recently emerged as a more efficient catalyst than the Cu–ZSM-5 for low-temperature applications such as diesel engine exhaust (19). For example, the NO + C_2H_4 + O_2 reaction lights off at much lower temperatures on Pt–ZSM-5 than on Cu–ZSM-5, but with more N_2O formation (28, 29). The hydrothermal stability of Pt–ZSM-5 has been reported to be much better than that of Cu–ZSM-5 (19, 28). In view of these different characteristics of Pt–ZSM-5 compared with Cu–ZSM-5, it is desirable to gain a better understanding of the catalytic activity of Pt–ZSM-5 for its practical application in lean NO_x control.

The phenomena of autonomous kinetic oscillation in heterogeneous catalytic reaction systems have been reported in the literature for a variety of reaction system (30–32). Among the well-known examples are oxidation of CO, hydrogen, or hydrocarbons on noble metals (32–37) and NO + CO reaction on noble metals (38–41). These kinetic oscillations have often been used as a tool to elucidate a detailed kinetic mechanism of the reactions (e.g., 30, 42, 43). A common feature of these reaction systems exhibiting self-sustained spontaneous kinetic oscillation is that they are all oxidizing reactions. In this connection, it is useful to recognize the unique feature of the so-called lean-NO_x reduction process in which the NO reduction proceeds as a subreaction in an overwhelmingly oxidizing environment due to a large excess amount of oxygen. In the lean-NO_x reduction process, which involves NO, O_2, and hydrocarbons, kinetic oscillations have not been reported in the literature.

In this work, we report spontaneous, sustained kinetic oscillations observed during the NO + C_2H_4 + O_2 reaction over a Pt–ZSM-5 catalyst under steady-state feed conditions in the presence of a large amount of excess oxygen. To the best of our knowledge, this is the first instance of such an observation in lean-NO_x catalysis. Based on our observations, we discuss the mechanism of the lean-NO_x catalysis on Pt–ZSM-5 and propose a few plausible kinetic mechanisms that may explain this very unusual kinetic behavior.

EXPERIMENTAL

The ZSM-5 zeolite obtained from PQ Corp. had a high Si/Al ratio of 40. The Pt–ZSM-5 catalyst was made from ion exchange of Pt on the ZSM-5 zeolite using $Pt(NH_3)_4Cl_2$ salt as the Pt ion precursor. The Pt loading was 5.9 wt%, which corresponds to a Pt/Al ratio of 0.74. After drying overnight at room temperature and then calcining in flowing air for 4 h at 500°C, this Pt–ZSM-5 powder was made into a disk by being compressed at 10 ton pressure. The

[1] To whom correspondence should be addressed.
[2] Present address: Ajou University, Suwon, Korea.

0021-9517/95 $12.00

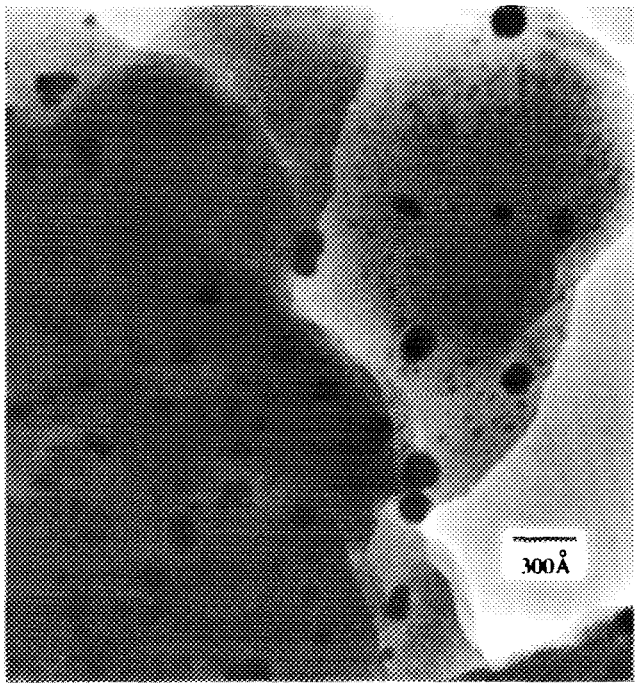

FIG. 1. Pt particles on ZSM-5 measured by TEM after *ex situ* aging at 400°C under the standard reaction conditions.

resulting Pt–ZSM-5 disk was crushed, ground, and screened to 80–120 mesh sizes for use in reactor experiments.

The reactor was made of a 0.32-cm-o.d. stainless-steel tube packed with the Pt–ZSM-5 powder. Before each experimental run for activity measurement, the catalyst was pretreated with oxygen for 2 h at 600°C. Shown in Fig. 1 are Pt particles on ZSM-5 measured by TEM after the catalyst sample was pretreated with oxygen for 2 h at 600°C followed by aging *ex situ* at 400°C for 98 h under the standard reaction conditions (i.e., $C_{C_2H_4}$ = 1200 ppm, C_{NO} = 230 ppm, and C_{O_2} = 7% under helium). Interestingly, the Pt particle size distribution exhibits a distinctly biomodal distribution. The average size of large Pt particles clearly shown in Fig. 1 is about 8 nm, and they must be outside the zeolite micropores. Note that the maximum size of the Pt particles that can be located inside the ZSM-5 pore structure is supposed to be around 1 nm, the size of the channel intersection. The average size of the small Pt particles shown mostly in the upper-right-hand corner of Fig. 1 is about 1 nm, and apparently they are within the micropore structure of ZSM-5.

The reactor temperature was measured at the inlet of the catalyst bed and controlled electronically with a typical precision of ±1°C. The reactor temperatures measured at the reactor outlet were nearly identical (within 2°C difference) with the inlet temperature under all experimental conditions, indicating that the gas-phase temperature of the reactor remained essentially isothermal. This appears to be due to the large thermal capacity of the reactor assembly, which contains an extremely small amount of the catalyst sample, in combination with a very low level of the reactant concentrations and a very large space velocity. The gas flow rate through the reactor was measured and controlled by electronic mass flow controllers. Transient responses of the gas-phase concentration in the exit stream from the reactor were monitored as a function of time by a mass spectrometer. Mass number 26 was used for a secondary mass peak of ethylene to prevent interference between the principal mass peak of ethylene (mass number = 28) and that of CO (mass number = 28). Isotopic ^{15}NO was used in place of regular ^{14}NO to distinguish CO_2 (mass number = 44) from $^{15}N_2O$ (mass number = 46) in the mass spectrometer signal. For simplicity in notation, NO will be used for ^{15}NO throughout this paper unless the full notation is required for clarity. Details of the standard experimental conditions are listed in Table 1.

RESULTS

General Pattern of Self-Sustained Spontaneous Oscillation of NO + C_2H_4 + O_2 Reaction over Pt–ZSM-5

Figures 2a and 2b show interesting patterns of the self-sustained spontaneous oscillation of gas-phase concentrations, measured by a mass spectrometer at the reactor outlet during the NO + C_2H_4 + O_2 reaction over Pt–ZSM-5 under steady feed conditions. The feed concentration ratio of NO to C_2H_4 was 0.228, and the reactor inlet temperature was kept at 200°C. During the early stage of the reaction (Fig. 2a), the kinetic oscillation of the gas-phase concentration occurs almost in a square-wave pattern, with

TABLE 1

Standard Experimental Conditions

Reactor
0.32-cm-o.d. stainless-steel tubing
Catalyst = Pt–ZSM-5 powder
Si/Al ratio = 40
Pt loading = 5.9 wt%
Particle size = 80–120 mesh
Sample weight = 0.0016 g
Catalyst bed length = 0.1 cm
Gas flow rate = 50 cm^3/min
Gas space velocity = 859,000 h^{-1}
Temperature = 100–500°C
Pressure = 101.3 kPa (1 atm)
Feed Concentration
C_2H_4 = 860–1200 ppm
O_2 = 7%
NO = 0–300 ppm
He = balance

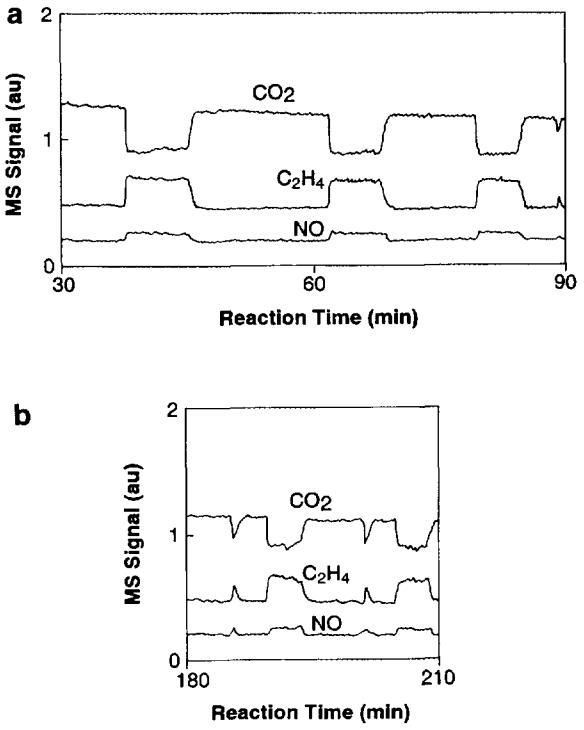

FIG. 2. Typical patterns of the steady-state kinetic oscillation measured by the gas-phase concentration at the reactor exit ((a) early stage of the reaction, (b) stabilized reaction, $C_{NO}/C_{C_2H_4} = 0.228$, $C_{NO} = 197$ ppm, $C_{C_2H_4} = 864$ ppm, $C_{O_2} = 7\%$, $T = 200°C$).

the oscillation period decreasing with reaction time. The oscillating concentration waves of NO, C_2H_4, and CO_2 species are exactly in phase, as expected from the reaction stoichiometry. Figure 2b shows the stabilized pattern of the oscillation after 3 h, which is distinctly a double-mode oscillation.

Effect of Temperature on the Pattern of Oscillation

Presented in Figs. 3a through 3c are the effects of catalyst temperature on the oscillating pattern of the NO + C_2H_4 + O_2 reaction over Pt–ZSM-5, when the feed concentrations of NO and C_2H_4 were kept constant at 270 and 1030 ppm, respectively. The reaction time shown on the x axis was measured after the oscillation was stabilized. At 197°C (Fig. 3a), the catalyst activity oscillates primarily in a triple mode with an oscillating period of approximately 16.2 min. The oscillation amplitude of the catalytic activity appears to be confined between the low and high activity levels, although it varies with time within each oscillation period. At 203°C (Fig. 3b), the oscillation pattern assumes a primary double mode interspersed with a triple mode. The catalytic activity is mostly in the high activity level with periodic loss of its activity for a very short period of time. At 210°C (Fig. 3c), the oscillation period becomes very long (approximately 1.5 h), and no oscillation was

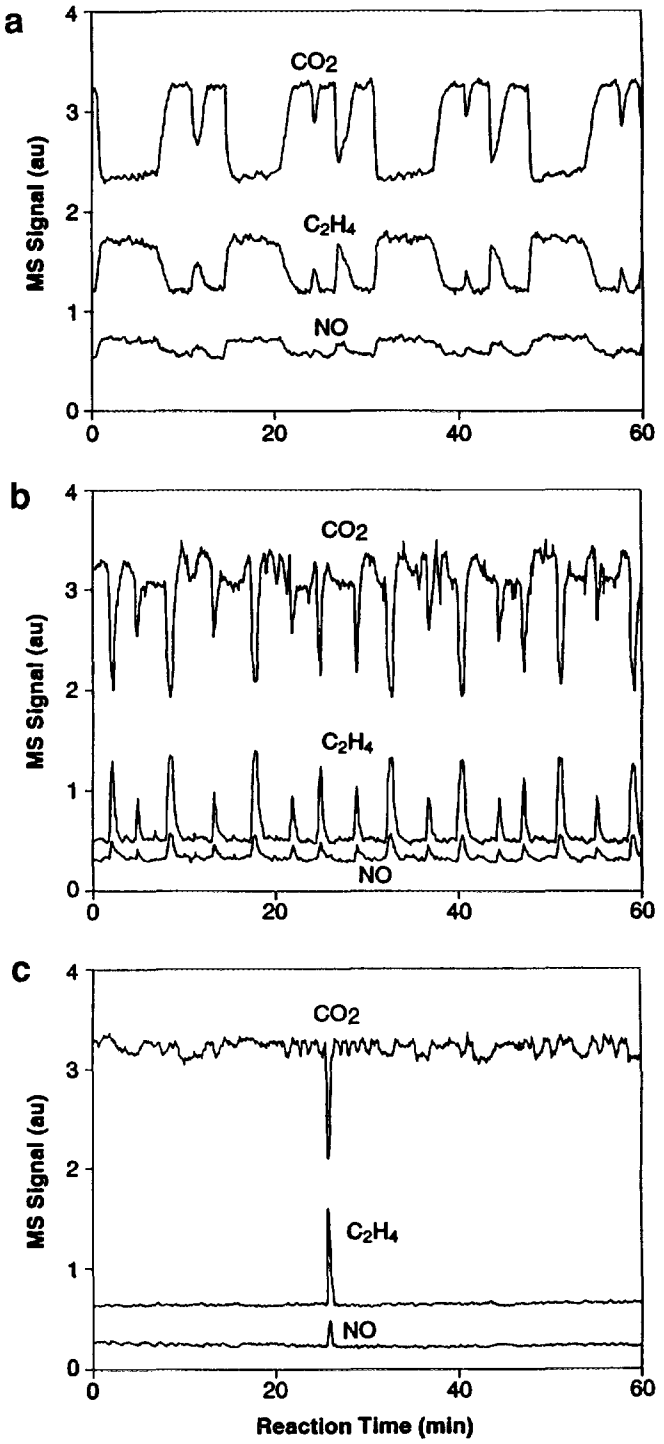

FIG. 3. Effect of catalyst temperature on the oscillation pattern ($C_{NO} = 270$ ppm, $C_{C_2H_4} = 1030$ ppm, $C_{O_2} = 7\%$; (a) $T = 197°C$; (b) $T = 203°C$; (c) $T = 210°C$).

observed above this temperature. Under the experimental conditions considered in these experiments, the temperature range over which the oscillation occurs was found to be between 195 and 210°C.

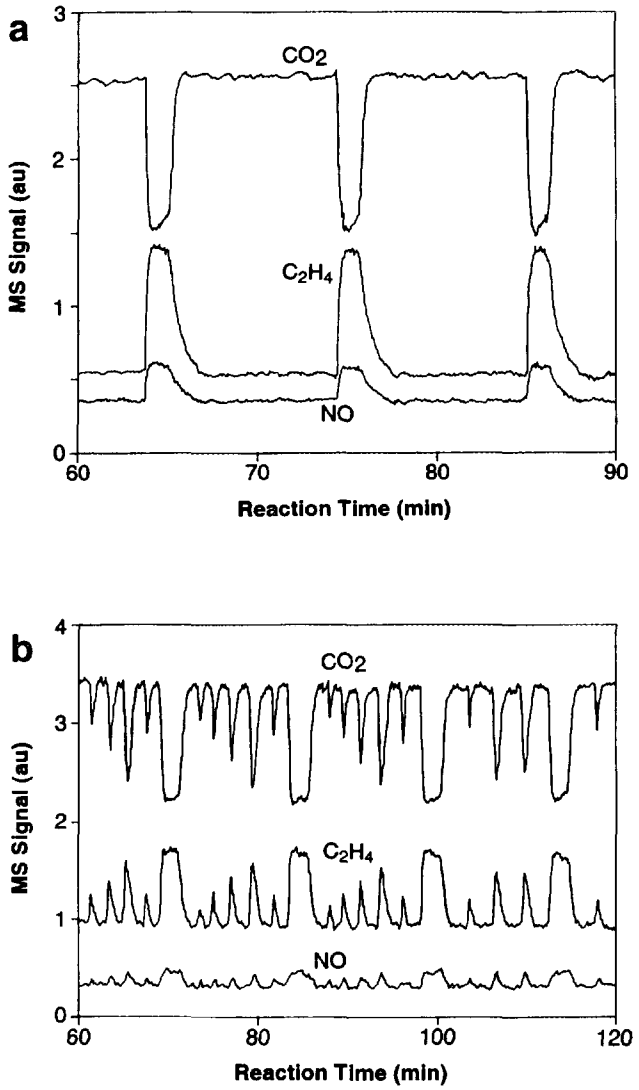

FIG. 4. Effect of feed composition on the oscillation pattern (T = 200°C, C_{O_2} = 7%; (a) $C_{NO}/C_{C_2H_4}$ = 0.261, C_{NO} = 265 ppm, $C_{C_2H_4}$ = 1016 ppm; (b) $C_{NO}/C_{C_2H_4}$ = 0.192, C_{NO} = 230 ppm, $C_{C_2H_4}$ = 1200 ppm).

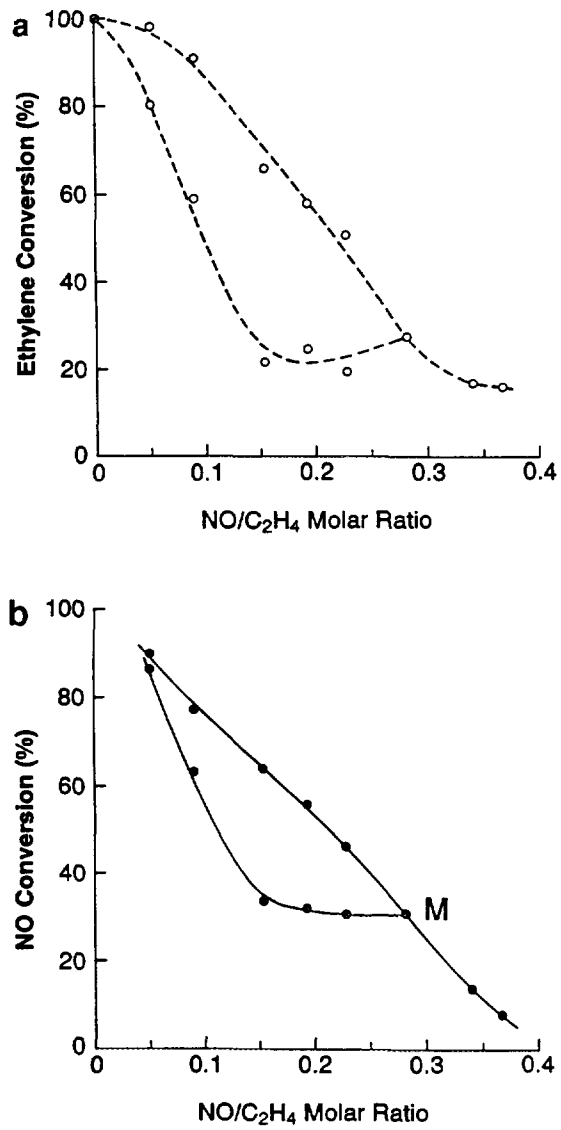

FIG. 5. Bifurcation diagram for the kinetic oscillation ((a) C_2H_4 conversion, (b) NO conversion, T = 200°C, $C_{C_2H_4}$ = 860 ppm, C_{NO} = variable).

Effect of Feed Composition on the Pattern of Oscillation

The effect of feed composition on the oscillation pattern was examined by varying the feed concentrations of both NO and C_2H_4 while keeping all the other experimental conditions the same. Results presented in Figs. 4a and 4b are the stabilized oscillation patterns for two different feed concentration ratios of NO to C_2H_4 at 200°C, where the reaction time was measured from the start of the reaction. Note the dramatic changes in the oscillation mode due to the change in feed composition; the oscillation is in a single mode when the concentration ratio is 0.261 (C_{NO} = 265 ppm, $C_{C_2H_4}$ = 1016 ppm), as shown in Fig. 4a, whereas it becomes a multiple mode when the ratio becomes 0.192 (C_{NO} = 230 ppm, $C_{C_2H_4}$ = 1200 ppm), as shown in Fig. 4b. Also noteworthy is the increase of the oscillation period in Fig. 4b compared with that in Fig. 4a.

Bifurcation Diagram

Presented in Figs. 5a and 5b are experimental bifurcation diagrams for the stabilized oscillation at 200°C where the maximum and minimum conversion levels are shown for both NO and C_2H_4 conversions within the oscillation regime, while the unique steady-state conversion levels are shown outside the oscillation regime. The molar feed ratio

of NO to C_2H_4 was varied by changing the NO feed concentration while keeping the C_2H_4 feed concentration constant at 860 ppm. It is clear in the figures that the presence of NO inhibits the conversions of both C_2H_4 and NO and that the rate of the NO + C_2H_4 + O_2 reaction decreases with increasing NO concentration. In view of the small values of the molar feed ratio of NO to C_2H_4 covered in Fig. 5, the C_2H_4 conversion is considered due primarily to the oxidation of C_2H_4 by oxygen. The kinetic oscillation occurs in a range of NO/C_2H_4 molar ratios between 0 and 0.28 at 200°C, whereas unique steady-state kinetics are observed above 0.28. The NO conversion at the bifurcation point M in Fig. 5b is 31.1%, which corresponds to a turnover frequency (TOF) of 5.4×10^{-3} s^{-1} based on the total Pt loading. In the absence of NO (i.e., the NO/C_2H_4 molar ratio of zero), there was no kinetic oscillation. This suggests that the kinetic oscillation in the NO + C_2H_4 + O_2 system over Pt–ZSM-5 occurs due to the presence of NO. Note also that the regime of kinetic oscillation for C_2H_4 conversion matches that for NO.

Kinetic Isotope Effect

We examined the possibility of kinetic isotope effects by replacing ^{15}NO with ^{14}NO in the ^{15}NO + C_2H_4 + O_2 reaction system while maintaining all other conditions the same. Results are shown in Figs. 6a and 6b as a function of temperature for both the ^{14}NO + C_2H_4 + O_2 and ^{15}NO + C_2H_4 + O_2 systems. In the case of the ^{15}NO + C_2H_4 + O_2 system, the lower bifurcation point is denoted by P and the upper one by Q for both NO and C_2H_4 conversion profiles. The confined area between P and Q, bounded by the maximum and minimum conversions as well as by the upper and lower bifurcation temperatures, indicates the region of the kinetic oscillations. In Figs. 6a and 6b, two interesting phenomena can be observed. One is that the ^{14}NO + C_2H_4 + O_2 system did not yield the kinetic oscillation, whereas kinetic oscillations were observed for the ^{15}NO + C_2H_4 + O_2 system under exactly the same experimental conditions. The other is that the lightoff temperature for the ^{15}NO + C_2H_4 + O_2 reaction (defined as the temperature required for 50% conversion of C_2H_4) is about 10°C higher than that for the ^{14}NO + C_2H_4 + O_2 reaction. Obviously, the inhibition effect of ^{15}NO is greater than that of ^{14}NO on the rate of the NO + C_2H_4 + O_2 reaction, suggesting that the kinetic oscillation may be closely related to the strong inhibition effect of ^{15}NO. This strong kinetic isotope effect appears to be a unique kinetic characteristic of the nitric oxide reduction by hydrocarbons over Pt–ZSM-5 catalysts under highly lean conditions. It is also noteworthy that the amplitude of oscillation increases with temperature up to a critical value, above which the kinetic oscillations disappear. This pattern of the bifurcation in temperature is quite different from that observed in Figs. 5a and 5b for the bifurcation in concentration.

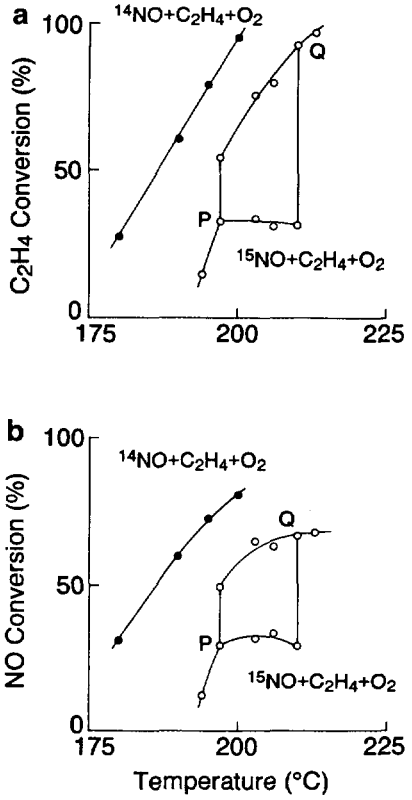

FIG. 6. Kinetic isotope effects on the conversion of ethylene and NO (C_{NO} = 230 ppm, $C_{C_2H_4}$ = 1200 ppm, C_{O_2} = 7%; (a) ethylene conversion; (b) NO conversion; (○) ^{15}NO + C_2H_4 + O_2, (●) ^{14}NO + C_2H_4 + O_2).

DISCUSSION

To the best of our knowledge, kinetic oscillations in the NO + C_2H_4 + O_2 reaction system under highly oxidizing conditions have not been reported in the literature. The kinetic oscillation observed in this study is essentially a relaxation-type oscillation which is characterized by a rapid change in the reaction rate at the beginning of the oscillation cycle followed by a slow relaxation to the original state (30). In the following, we will discuss the important aspects of the NO + C_2H_4 + O_2 reaction kinetics on Pt–ZSM-5, culminating in the discussion of the mechanism of the kinetic oscillation.

Inhibition Effect of NO on the Rate of NO + C_2H_4 + O_2 Reaction

We have demonstrated experimentally that the presence of NO inhibits the rate of C_2H_4 oxidation by O_2. Although similar inhibition effects of NO were reported previously for the oxidation of CO and C_3H_6 on Pt/Al_2O_3 (44), it is

surprising to see in this work that such a small amount of NO (as little as 40 ppm) can significantly inhibit the oxidation rate of C_2H_4 in the presence of such a large amount of excess O_2 (as much as 7%). The mechanism of this inhibition effect of NO can be explained as follows, by recognizing two important facts regarding the interaction of NO and O_2 with the catalytic surface. First, NO competes effectively with O_2 for dissociative adsorption sites on Pt surface (45); second, the dissociation rate of adsorbed NO is slower than that of adsorbed oxygen on polycrystalline Pt surfaces (46). In other words, NO is a much less efficient oxidant than O_2 on Pt surfaces. Therefore, any NO adsorbed at the expense of adsorbed oxygen will decrease the rate of C_2H_4 oxidation, either by blocking the active sites or as a result of a limited supply of oxygen atoms on the surface. This competitive adsorption mechanism is consistent with the rate expression reported previously on a propylene oxidation system (44).

The decreasing rate of C_2H_4 oxidation with increasing NO concentration is always accompanied by the decreasing rate of NO reduction. This suggests that the C_2H_4 oxidation rate is closely related to the NO reduction rate. Based on the competitive adsorption mechanism, this can be explained as follows. The increasing rate of C_2H_4 oxidation increases the rate of regeneration of vacant catalytic sites by scavenging oxygen and C_2H_4 from the catalytic surface, thereby increasing the probability of NO adsorbing and dissociating on the catalytic surface, and vice versa.

Mechanism of NO + C_2H_4 + O_2 Reaction over Pt–ZSM-5

The above discussions are consistent with a reaction mechanism for the NO + C_2H_4 + O_2 reaction, in which oxygen scavenging by C_2H_4 proceeds in parallel with NO dissociation on active catalytic surfaces. A similar reaction mechanism was proposed previously for Cu–ZSM-5 (11, 47, 48) and for Pt–ZSM-5 (48). Note that a reaction mechanism in which the NO_2 intermediate (formed via NO + O_2 reaction) reacts with hydrocarbons (15, 24) is not consistent with the inhibition effect of NO observed in this study. Based on our proposed reaction mechanism, which is a combination of NO dissociation and hydrocarbon oxidation, we speculate that any catalytic material which exhibits good activity toward both hydrocarbon oxidation and NO dissociation should be able to effectively reduce NO under lean conditions. Obviously, the effectiveness of the catalyst in terms of its selectivity toward NO reduction under highly oxidizing conditions may vary depending upon the catalyst's unique kinetic characteristics. Our conjecture does seem to be consistent with literature reports published so far.

Kinetic Isotope Effect

One of the most interesting kinetic phenomena observed in this study is a strong kinetic isotope effect which revealed that a mere change of a reactant from ^{15}NO to ^{14}NO not only eliminates the kinetic oscillations but also increases the overall reaction rate under the same reaction conditions. This unusually strong kinetic isotope effect may be explained by the combination of the primary and secondary isotope effects: the primary effect is defined here as the isotope effect on the intrinsic rate of NO dissociation, while the secondary effect is due to the inhibition effect exerted by the increased surface coverage of NO resulting from the primary isotope effect.

It has been shown that ^{15}NO adsorbed on Pt surfaces is characterized by lower vibration frequencies than ^{14}NO (49). This means that the molecular bond in ^{15}NO absorbs less energy than that in ^{14}NO, since the amount of energy absorbed is proportional to the vibrational frequency. This in turn means that the thermal activation of the stretching vibration of ^{15}NO molecules on Pt is more difficult than that of ^{14}NO, indicating that ^{15}NO requires a greater activation energy for its dissociation than ^{14}NO. In other words, the dissociation of ^{15}NO on Pt surfaces is more difficult than that of ^{14}NO. This is consistent with the earlier observation that the ^{15}NO + C_2H_4 + O_2 reaction has a higher lightoff temperature than the ^{14}NO + C_2H_4 + O_2 reaction (Figs. 6a and 6b). It is also consistent with the results of earlier ammonia dissociation experiments (50, 51) which have shown that ND_3 dissociates slower than NH_3 on both Co and Cu surfaces, in the sense that the heavier isotopic molecule exhibits the slower dissociation rate.

For a quantitative analysis of the primary isotope effect, we note that the vibration frequency of ^{15}NO adsorbed on Pt surfaces can be calculated from the vibration frequency of ^{14}NO by

$$\frac{\nu'}{\nu} = \sqrt{\frac{\mu}{\mu'}}, \qquad [1]$$

where ν (or ν') and μ (or μ') are the vibrational wavenumber and the reduced mass of ^{14}NO (or ^{15}NO), respectively. The dissociation rate constant of ^{15}NO can then be calculated from that of ^{14}NO using the information on the vibrational wavenumber (52) by

$$\frac{k'}{k} = \sinh\left(\frac{hc\nu'}{2\kappa T}\right) \Big/ \sinh\left(\frac{hc\nu}{2\kappa T}\right), \qquad [2]$$

where k and k' denote the dissociation rate constants of ^{14}NO and ^{15}NO, respectively, and the definitions of other notations can be found in Appendix A. With the vibrational wavenumber of ^{14}NO on Pt surfaces at 1780 cm^{-1} (49), Eq. [2] with the help of Eq. [1] yields

$$k'/k = 0.93, \qquad [3]$$

indicating that the dissociation rate of ^{15}NO is slower than that of ^{14}NO by approximately 7%. Obviously, this primary effect alone cannot adequately explain the strong isotope effect observed in Fig. 6b.

The secondary isotope effect comes from the increased surface coverage of NO resulting from the slow dissociation rate of ^{15}NO (compared with that of ^{14}NO), and it can make a significant contribution to the decrease in the overall reaction rate. Recently, it has been shown that this secondary effect is a more important factor than the primary effect in reducing the overall reaction rate and that the combination of the primary and the secondary effects can adequately explain the kinetic isotope effects observed in this paper (53). Detailed analysis of the secondary effect is beyond the scope of this paper and will be treated in a subsequent paper.

Based on the above discussions, we conclude that ^{15}NO exerts a greater inhibition effect than ^{14}NO on the rate of the NO + C_2H_4 + O_2 reaction and that the smaller inhibition effect of ^{14}NO may not be sufficient to reach the threshold value needed to initiate the oscillation cycle. This kinetic isotope effect also strongly suggests that the kinetic oscillation is due primarily to the NO-related kinetics such as NO dissociation.

Mechanism of Steady-State Kinetic Oscillation

In the absence of an established kinetic expression and the associated kinetic parameter values for the lean-NO_x catalysis, any quantitative analysis of the kinetic oscillations observed in this work does not seem to be feasible at this point. However, even though the exact mechanism of the kinetic oscillations is not yet clearly understood, we propose, as a first step toward better understanding of this interesting phenomenon, two plausible mechanistic models that may explain at least qualitatively the observed kinetic oscillations. In one model we focus on the catalytic activity of Pt for NO dissociation, while in another we focus on the inhibition effect of NO, as will be described in the following.

1. Surface phase-transition model. It is well documented that Pt(100) is the most stable plane on polycrystalline and supported Pt particles (54, 55) and that it undergoes phase transition from the (hex) to the (1 × 1) phase, induced by the adsorption of NO (56–58). The (1 × 1) phase is known to be much more active than the (hex) phase for NO dissociation (59, 60), and hence it is more active for the NO + CO reaction than the (hex) phase. It now appears that the adsorbate-induced surface phase transition between the (1 × 1) and the (hex) phases is of great importance not only for the kinetics of NO dissociation but also for the kinetics of lean-NO_x reduction.

The surface phase-transition model can be applied to the lean-NO_x reduction system to qualitatively explain the observed kinetic oscillation as follows. Upon the transition of the Pt surface from the (1 × 1) to the (hex) phase, the rate of NO dissociation becomes very slow on the (hex) phase and the surface coverage of NO (θ_{NO}) starts to increase, resulting in a decrease in the C_2H_4 oxidation rate due to the increased inhibition effect of NO on the surface. When θ_{NO} reaches the upper critical value, the phase transition from the (hex) to the (1 × 1) phase occurs. The rate of NO dissociation on the restored (1 × 1) phase becomes very fast, resulting in a decrease of the NO coverage on the surface, which in turn leads to an increase of the C_2H_4 oxidation rate due to the decreased NO inhibition effect. On reaching the lower critical value of θ_{NO}, the phase transition from the (1 × 1) to the (hex) occurs, completing the periodic process. Note that similar phase-transition models, used previously to explain kinetic oscillations in both the (NO + CO) reaction (59) and the (CO + O_2) reaction system (61, 62), do not have the synergistic effect between the phase-transition and the NO inhibition effect as described above.

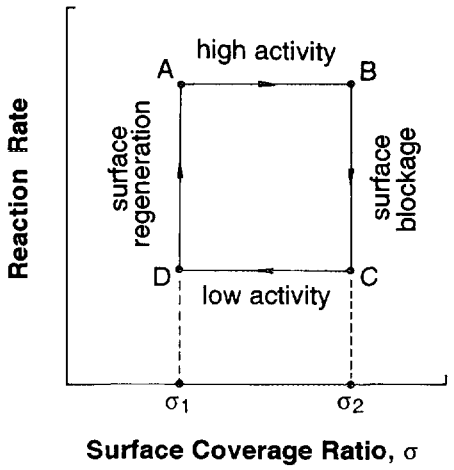

FIG. 7. Schematic diagram of the kinetic oscillation process based on the surface regeneration model.

2. Surface regeneration model. The observed kinetic oscillation can also be explained by the inhibition effect of NO in combination with the competitive adsorption of reactant species on the catalytic surface, as illustrated schematically in Fig. 7. Path AB in Fig. 7 represents a high-activity state, while path CD represents a low-activity state of the catalyst. Paths BC and DA denote the transitions between these two states through surface blockage and surface regeneration, respectively. The arrows point to the direction of time. The ratio of surface coverage, $\theta_{NO}/\theta_{C_2H_4}$, denoted by σ on the x axis, physically represents the ratio of the reaction inhibitor (i.e., NO) to the reaction promoter (i.e., C_2H_4) on the catalytic surface. Oxygen can be treated as a neutral species, for it promotes the ethylene oxidation but inhibits the dissociation of NO.

At point A, the catalyst is in a state in which C_2H_4 oxidation occurs at a high rate. This high rate of C_2H_4 oxidation indicates the high rate of scavenging both oxygen and C_2H_4 from the catalytic surface, making more vacant sites available for NO adsorption. As a result, NO coverage increases relative to oxygen and ethylene coverages on the catalytic surface. Thus, the surface coverage ratio (σ) increases along the path from A to B. At point B, the upper threshold ratio (σ_2) on the surface is reached and a further increase in the ratio abruptly decreases the reaction rate due to the overwhelming effect of the inhibition by NO, leading the catalyst to the low-activity state.

At point C, the catalyst is in a low-activity state with a high surface coverage ratio. Along the path from C to D, the rate of scavenging oxygen and ethylene from the catalytic surface is slow compared with that along the path from A to B. As a result, the surface coverages of oxygen and ethylene increase relative to that of NO along the path from C to D, thereby reducing the surface coverage ratio. Eventually, the lower threshold ratio (σ_1) is reached at point D, where the transition from the low-activity to the high-activity state occurs due to the combination of the decreased inhibition effect of NO and the increased promotional effect of ethylene. Previously, a similar model based on the vacant site requirement for NO dissociation has been proposed to explain the kinetic oscillation of the (NO + CO) reaction over the Pt(100) surface (39).

It is possible that both the surface phase-transition process and the surface regeneration process contribute to the kinetic oscillations observed in this study. However, we speculate that the surface phase-transition model may not be applicable to the very small Pt particles located inside the zeolite micropores, considering the limited number of surface atoms available for the phase transition.

The reason that the ordinary ^{14}NO does not lead to the kinetic oscillation is not clearly understood at this time, but we propose the following explanation. As shown in Figs. 6a and 6b, the rate of ^{14}NO conversion is faster than that of the isotopic ^{15}NO conversion at the same temperature. This can be attributed to the difference in the dissociation rate between ^{14}NO and ^{15}NO, as discussed earlier. In the case of the surface regeneration model, if the dissociation rate of ^{14}NO is faster than that of ^{15}NO to the extent that the inhibition effect of ^{14}NO is not strong enough to reach the threshold value of σ_2 (i.e., point B in Fig. 7), the catalyst will stay in the high-activity state and the kinetic oscillation cannot occur. A similar argument may also be applicable to the surface phase-transition model. Another possible explanation for the different behavior between ^{14}NO and ^{15}NO may be that the impurities contained in each nitric oxide gas tank might be different (e.g., NO_2, N_2O, etc), which might in turn give rise to different behavior as was observed here. However, we are inclined to discount this possibility because the impurity levels were unmeasurably small (as detected by the mass spectrometer) for both ^{14}NO and ^{15}NO gas tanks: The upper bound of any impurity was 3 ppm under our experimental conditions.

The above discussions indicate that the NO inhibition effect is a very important factor in understanding the kinetic mechanism of lean NO_x reduction. It needs to be emphasized that this inhibition effect by NO is directly related to the dissociation rate of NO itself. The faster the dissociation rate of NO, the smaller the inhibition effect by NO on the rate of the NO + C_2H_4 + O_2 reaction. Other factors such as pore diffusion resistance and nonuniform temperature distribution in the catalyst particles may also have contributed to the detailed structure of the kinetic oscillation observed here. However, in view of the strong kinetic isotope effect discussed earlier, these additional factors are not expected to affect our general conclusions because these macroscopic physical as well as spatiotemporal effects are believed to be independent of the isotopic substitution in the NO molecule. Particularly, the internal diffusion resistance is considered to be negligible under our experimental conditions, according to a detailed analysis presented in Appendix B.

SUMMARY AND CONCLUSIONS

To elucidate the kinetic mechanism of NO reduction by hydrocarbons in the presence of excess oxygen, steady-state kinetics of a Pt–ZSM-5 catalyst was investigated for the NO + C_2H_4 + O_2 reaction using a packed-bed laboratory reactor under highly oxidizing conditions, typical of lean-burn gasoline engine exhaust. For the first time, we observed spontaneous, sustained oscillations in the rate of the NO + C_2H_4 + O_2 reaction. Effects of feed composition and catalyst temperature on the behavior of the kinetic oscillations were also investigated. The reaction mechanisms of NO reduction are discussed in light of the observed kinetic oscillations, and two possible mechanisms for the kinetic oscillations are proposed. The important findings are listed below.

1. The rate of the NO + C_2H_4 + O_2 reaction over Pt–ZSM-5 is inhibited by the presence of NO. This observation argues against one of the reaction mechanisms proposed in the literature, in which a reaction intermediate NO_2, formed via the NO + O_2 reaction, subsequently oxidizes the hydrocarbon.

2. Only in the presence of NO did spontaneous kinetic oscillations occur in the temperature range of 195–210°C. This suggests that the kinetic oscillation is induced by the presence of NO.

3. Switching between ^{14}NO and ^{15}NO in the feed stream affects substantially the steady-state activity of the Pt–ZSM-5 catalyst, indicating significant kinetic isotope effects.

4. The steady-state kinetic oscillation can be qualitatively explained by the surface phase-transition model and/or by the surface regeneration model.

The spontaneous kinetic oscillation in a lean-NO_x catalyst system described here is an interesting new phenomenon which has not been reported in the literature. It is hoped that our discovery of this new phenomenon will help us to unravel the reaction mechanism of NO reduction under lean-burn engine exhaust conditions.

APPENDIX A: NOMENCLATURE

c = speed of light, 2.9979×10^{10} cm/s
C = concentration of ethylene in the reactor, mol/cm^3
$C_{C_2H_4}$ = feed concentration of ethylene, ppm
C_{NO} = feed concentration of NO, ppm
C_{O_2} = feed concentration of oxygen, vol%
D_M = diffusivity of ethylene in macropores, cm^2/s
D_μ = diffusivity of ethylene in micropores, cm^2/s
h = Planck constant, 6.6256×10^{-27} erg · s
k, k' = dissociation rate constant of ^{14}NO and ^{15}NO, respectively, s^{-1}
k_r = reaction rate constant for ethylene conversions, s^{-1}
L = total reactor length, cm
r = average radius of microparticles, cm
R = average radius of macroparticles, cm
V = superficial linear gas velocity, cm/s
T = absolute temperature, K
x = fractional conversion of ethylene
z = axial distance along the reactor, cm

Greek Letters

ε = void fraction of the reactor bed
η = effectiveness factor of the catalyst
$\theta_{C_2H_4}$ = surface coverage of ethylene
θ_{NO} = surface coverage of NO
κ = Boltzmann constant, 1.3805×10^{-16} erg/K
μ, μ' = reduced mass of ^{14}NO and ^{15}NO, respectively, g
ν, ν' = vibrational wavenumber of ^{14}NO and ^{15}NO, respectively, cm^{-1}
σ = ratio of surface coverage defined by $\theta_{NO}/\theta_{C_2H_4}$
τ = residence time, s
τ_D = time constant for internal diffusion, s
τ_M, τ_μ = time constants for macropore diffusion and micropore diffusion, respectively, s
τ_R = time constant for ethylene conversion, s

APPENDIX B: EFFECT OF INTERNAL DIFFUSION RESISTANCE

To examine the effect of internal diffusion resistance on the observed reaction rate, we choose C_2H_4 as the representative reactant because it is the slowest diffusing species among reactants. As a criterion for the internal diffusion resistance, we compare the time constant for internal diffusion with that for reaction.

Time Constant for the Observed Reaction of C_2H_4

Assuming a first-order reaction for C_2H_4 conversion, a steady-state mass balance for C_2H_4 in a plug flow reactor under isothermal conditions can be written as

$$\varepsilon V \frac{dC}{dz} = -\eta k_r C, \qquad [B.1]$$

where C, k_r, and η are the C_2H_4 concentration, the reaction rate constant, and the effectiveness factor of the catalyst, respectively. Integration of Eq. [B.1] yields

$$\eta k_r = -\frac{\varepsilon V}{L} \ln(1 - x). \qquad [B.2]$$

The time constant for the observed conversion of C_2H_4 is then

$$\tau_R = 1/(\eta k_r) = -\tau/\ln(1 - x), \qquad [B.3]$$

where τ is the residence time, and x is the conversion of C_2H_4. Equation [B.3] indicates that τ_R decreases monotonically with the increasing conversion of C_2H_4. This means that the minimum value of τ_R can be obtained from the maximum observed conversion of C_2H_4. Using the maximum C_2H_4 conversion of 0.98 as shown in Fig. 5a, the minimum value of τ_R was calculated to be 4.3×10^{-4} s. In other words,

$$\tau_R \geq 4.3 \times 10^{-4} \text{ s}. \qquad [B.4]$$

Time Constant for Internal Diffusion

The catalyst particles (or macroparticles) employed in this study are aggregates of small microparticles of ZSM-5. The average radii of the microparticles (r) and the macroparticles (R) are about 0.5 and 75 μm, respectively. There are two kinds of pores within the macroparticle structure: macropores between individual microparticles, and micropores within each microparticle. Diffusion through the macropores is primarily molecular diffusion, since the average size of the macropores is typically in the range of the microparticle size, which is much greater than the mean free path. Thus, the diffusion coefficient of C_2H_4 through the macropores (D_M) can be estimated from the Wilke–Lee correlation (63) to obtain

$$D_M = 1.2 \text{ cm}^2/\text{s} \quad \text{at } 200°\text{C}. \qquad [B.5]$$

Diffusion through the micropores is configurational diffu-

sion, since the size of the micropores in ZSM-5 is about 0.55 nm, which is close to the size of C_2H_4 molecules. In the absence of available data, the diffusion coefficient of C_2H_4 through the micropores of ZSM-5 (D_μ) can be estimated from that of C_2H_6 (64) to yield

$$D_\mu = 8.5 \times 10^{-5}\ \text{cm}^2/\text{s} \quad \text{at } 200°\text{C}. \qquad [B.6]$$

Using these values, the time constants for macropore diffusion (τ_M) and micropore diffusion (τ_μ) can be calculated to obtain

$$\tau_M = R^2/(9D_M) = 5.2 \times 10^{-6}\ \text{s}, \qquad [B.7]$$

$$\tau_\mu = r^2/(9D_\mu) = 3.3 \times 10^{-6}\ \text{s}. \qquad [B.8]$$

The overall time constant for C_2H_4 diffusion (τ_D) is then

$$\tau_D = \tau_M + \tau_\mu = 8.5 \times 10^{-6}\ \text{s}. \qquad [B.9]$$

Criterion for Internal Diffusion Resistance

The effect of the internal diffusion resistance can be evaluated by comparing the time constant for diffusion with that for reaction. That is, the internal diffusion resistance is negligible if the ratio (τ_D/τ_R) is much smaller than unity, whereas it becomes the limiting factor of the reaction rate if this ratio is much greater than unity. Under our experimental conditions, Eqs. [B.4] and [B.9] result in

$$\tau_D/\tau_R \leq 2.0 \times 10^{-2}, \qquad [B.10]$$

which is much smaller than unity. This indicates that the internal diffusion resistance is negligible under our experimental conditions.

ACKNOWLEDGMENTS

We thank Dr. N. A. Potter and Mr. M. P. Balogh of the Analytical Chemistry Department for chemical and TEM analyses of the Pt–ZSM-5 catalyst used in this study.

REFERENCES

1. Iwamoto, M., *in* "Future Opportunities in Catalytic and Separation Technology; Studies in Surface Science and Catalysis" (M. Misono, Y. Moro-oka, and S. Kimura, Eds.), Vol. 54. Elsevier, Amsterdam, 1990.
2. Held, W., Konig, A., Richter, T., and Puppe, L., SAE Paper 900496, 1990.
3. Iwamoto, M., and Hamada, H., *Catal. Today* **10,** 57 (1991).
4. Sato, S., Yu-u, Y., Yahiro, H., Mizuno, N., and Iwamoto, M., *Appl. Catal.* **70,** L1 (1991).
5. Montreuil, C. N., and Shelef, M., *Appl. Catal. B.* **1,** L1 (1992).
6. Li, Y., and Armor, J. N., *Appl. Catal. B* **1,** L31 (1992).
7. Zhang, G., Yamaguchi, T., Kawakami, H., and Suzuki, T., *Appl. Catal. B* **1,** L15 (1992).
8. Truex, T. J., Searles, R. A., and Sun, D. C., *Platinum Met. Rev.* **36,** 2 (1992).
9. Konno, M., Chikahisa T., Murayama, T., and Iwamoto, M., SAE Paper 920091, 1992.
10. Bennett, C. J., Bennett, P. S., Golunski, S. E., Hayes, J. W., and Walker, A. P., *Appl. Catal. A* **86,** L1 (1992).
11. Cho, B. K., *J. Catal.* **142,** 418 (1993).
12. Monroe, D. R., DiMaggio, C. L., Beck, D. D., and Matekunas, A., SAE Paper 930737, 1993.
13. Kharas, K. C. C., *Appl. Catal. B* **2,** 207 (1993).
14. Kharas, K. C. C., Robota, H. J., and Liu, D. J., *Appl. Catal. B* **2,** 225 (1993).
15. Ansell, G. P., Diwell, A. F., Golunski, S. E., Hayes, J. W., Rajaram, R. R., Truex, T. J., and Walker, A. P. *Appl. Catal. B* **2,** 81 (1993).
16. Burch, R., and Millington, P. J., *Appl. Catal. B* **2,** 101 (1993).
17. d'Itri, J. L., and Sachtler, M. H., *Appl. Catal. B* **2,** L7 (1993).
18. Obuchi, A., Ohi, A., Nakamura, M., Ogata, A., Mizuno, K., and Obuchi, H., *Appl. Catal. B* **2,** 71 (1993).
19. Engler, B. H., Leyrer, J., Lox, E. S., and Ostgathe, K., SAE Paper 930735, 1993.
20. Gopalakrishnan, R., Stafford, P. R., Davidson, J. E., Hecker, W. C., and Bartholomew, C. H., *Appl. Catal. B* **2,** 165 (1993).
21. Heinrich, M. J., and Deviney, M. L., SAE Paper 930736, 1993.
22. Li, Y., and Armor, J. N., *Appl. Catal. B* **2,** 239 (1993).
23. Li, Y., and Armor, J. N., *Appl. Catal. B* **3,** 55 (1993).
24. Petunchi, J. O., and Hall, W. K., *Appl. Catal. B* **2,** L17 (1993).
25. Petunchi, J. O., Sill, G., and Hall, W. K., *Appl. Catal. B* **2,** 303 (1993).
26. Ukisu, Y., and Sato, S., *Appl. Catal. B* **2,** 147 (1993).
27. Iwamoto, M., Yokoo, M., Sasaki, K., and Kagawa, S., *J. Chem. Soc. Faraday Trans.* **77,** 1629 (1981).
28. Iwamoto, M., Paper A-34 presented at the 13th North American Meeting of The Catalysis Society, Pittsburgh, PA, May 1993.
29. Cho, B. K., and Yie, J. E., unpublished results, General Motors NAO R&D Center, Warren, MI, 1994.
30. Sheintuch, M., and Schmitz, R. A., *Catal. Rev.-Sci. Eng.* **15,** 107 (1977).
31. Slin'ko, M. G., and Slin'ko, M. M., *Catal. Rev.-Sci. Eng.* **17,** 119 (1978).
32. Razon, L. F., and Schmitz, R. A., *Catal. Rev.-Sci. Eng.* **28,** 89 (1986).
33. Turner, J. E., Sales, B. C., and Maple, M. B., *Surf. Sci.* **103,** 54 (1981).
34. Kaul, D. J., and Wolf, E. E., *J. Catal.* **91,** 216 (1985).
35. Eiswirth, M., Moller, P., Wetzl, K., Imbihl, R., and Ertl, G., *J. Chem. Phys.* **90,** 510 (1989).
36. Sheintuch, M., and Luss, D., *J. Catal.* **68,** 245 (1981).
37. Kellow, J. C., and Wolf, E. E., *AIChE J.* **37,** 1844 (1991).
38. Adlhoch, W., Lintz, H.-G., and Weisker, T., *Surf. Sci.* **103,** 576 (1981).
39. Fink, Th., Dath, J.-P., Bassett, M. R., Imbihl, R., and Ertl, G., *Surf. Sci.* **245,** 96 (1991).
40. Fink, Th., Dath, J.-P., Imbihl, R., and Ertl, G., *J. Chem. Phys.* **95,** 2109 (1991).
41. Veser, G., and Imbihl, R., *J. Chem. Phys.* **96,** 7155 (1992).
42. Graham, W. R. C., and Lynch, D. T., *AIChE J.* **33,** 792 (1987).
43. Shanks, B. H., and Bailey, J. E., *Chem. Eng. Sci.* **44,** 901 (1989).
44. Voltz, S. E., Morgan, C. R., Liederman, D., and Jacob, S. M., *Ind. Eng. Chem. Prod. Res. Dev.* **12,** 294 (1973).
45. Mummey, M. J., and Schmidt, L. D., *Surf. Sci.* **109,** 29 (1981).
46. Lintz, H.-G., *Surf. Sci.* **108,** L486 (1981).
47. Cho, B. K., *J. Catal.* **155,** 184 (1995).
48. Burch, R., and Scire, S., *Appl. Catal. B* **3,** 295 (1994).
49. Morrow, B. A., Chevrier, J. P., and Moran, L. E., *J. Catal.* **91,** 208 (1985).
50. Iizuka, T., and Lunsford, J. H., *J. Am. Chem. Soc.* **100,** 6106 (1978).
51. Williamson, W. B., and Lunsford, J. H., *J. Phys. Chem.* **80,** 2664 (1976).
52. Melander, L., "Isotope Effects on Reaction Rates." Ronald Press, New York, 1960.

53. Cho, B. K., Yie, J. E., and Rahmoeller, K. M., Paper presented at 14th North American Meeting of The Catalysis Society, Snowbird, UT, June 1995.
54. Wang, T., Lee, C., and Schmidt, L. D., *Surf. Sci.* **163,** 181 (1985).
55. Schwartz, S. B., and Schmidt, L. D., *Surf. Sci.* **183,** L269 (1987).
56. Bonzel, H. P., Broden, G., and Pirug, G., *J. Catal.* **53,** 96 (1978).
57. Gardner, P., Tushaus, M., Martin, R., and Bradshaw, A. M., *Surf. Sci.* **240,** 112 (1990).
58. Veser, G., Esch, F., and Imbihl, R., *Catal. Lett.* **13,** 371 (1992).
59. Schwartz, S. B., and Schmidt, L. D., *Surf. Sci.* **206,** 169 (1988).
60. Lombardo, S. J., Fink, T., and Imbihl, R., *J. Chem. Phys.* **98,** 5526 (1993).
61. Ertl, G., Norton, P. R., and Rustig, J., *Phys. Rev. Lett.* **49,** 177 (1982).
62. Imbihl, R., Cox, M. P., Ertl, G., Muller, H., and Brenig, W., *J. Chem. Phys.* **83,** 1578 (1985).
63. Wilke, C. R., and Lee, C. Y., *Ind. Eng. Chem.* **47,** 1253 (1955).
64. Karger, J., and Ruthven, D. M., "Diffusion in Zeolites and Other Microporous Solids." Wiley, New York, 1992.